arXiv:1912.04847v1 [cond-mat.mes-hall] 10 Dec 2019

Electron transport through metal/MoS_2 interfaces: edge- or area-dependent process?

Áron Szabó[†], Achint Jain[‡], Markus Parzefall[‡], Lukas Novotny[‡], and Mathieu Luisier[†*]

[†] *Integrated System Laboratory, ETH Zürich, 8092 Zürich, Switzerland*

[‡] *Photonics Laboratory, ETH Zürich, 8093 Zürich, Switzerland*

E-mail: mluisier@iis.ee.ethz.ch

Phone: +41 44 632 53 33. Fax: +41 44 632 11 94

Abstract

In ultra-thin two-dimensional (2-D) materials, the formation of ohmic contacts with top metallic layers is a challenging task that involves different processes than in bulk-like structures. Besides the Schottky barrier height, the transfer length of electrons between metals and 2-D monolayers is a highly relevant parameter. For MoS_2, both short ($\leq$30 nm) and long ($\geq$0.5 μm) values have been reported, corresponding to either an abrupt carrier injection at the contact edge or a more gradual transfer of electrons over a large contact area. Here we use *ab initio* quantum transport simulations to demonstrate that the presence of an oxide layer between a metallic contact and a MoS_2 monolayer, for example TiO_2 in case of titanium electrodes, favors an area-dependent process with a long transfer length, while a perfectly clean metal-semiconductor interface would lead to an edge process. These findings reconcile several theories that have been postulated about the physics of metal/MoS_2 interfaces and provide a framework to design future devices with lower contact resistances.

Keywords: 2-D materials, metal-semiconductor interfaces, contact physics, transfer length, Fermi level pinning, *ab initio* device simulations

Transistors made of novel two-dimensional (2-D) materials beyond graphene such as single-layer MoS_2[1] have generated considerable excitement among the scientific community for their potential as active components of future integrated circuits. Transition metal dichalcogenides (TMDs),[2] black phosphorus,[3,4] and hundreds of other presumably exfoliable 2-D monolayers[5] appear as excellent candidates to outperform Si FinFETs, the current workhorse of the semiconductor industry, for next-generation ultra-scaled logic switches.[6] The advantages of 2-D materials over competing technologies reside in their naturally passivated surfaces, their planar geometry providing an excellent electrostatic control,[7] their exceptionally high carrier mobilities as compared to 3-D compounds with the same sub-nanometer thickness,[8–10] and the possibility of stacking them on top of each other to form van der Waals heterostructures.[11–13]

Before MoS_2 field-effect transistors (FETs) with a monolayer channel can reach their full potential and deliver the expected performance,[14] several key challenges remain to be solved. The source and drain contact resistances represent one of the main limiting factors as they usually lie in the $k\Omega \cdot \mu m$ range,[15,16] instead of 150 to 200 $\Omega \cdot \mu m$ as in conventional Si transistors [1]. Lower values have been reported with metalized 1T MoS_2[17] or nickel-etched graphene[18] electrodes, in the order of 200 $\Omega \cdot \mu m$, but for multilayer MoS_2. While top contacts are the most widely used variants due to their ease of fabrication, side contacts have started to emerge as a promising alternative,[19–22] motivated by theoretical studies that predict a stronger orbital overlap and shorter tunneling distances between metals and MoS_2 in lateral configurations.[23,24] Apart from the electrode geometry, other well-known techniques have been applied to reduce the contact resistance of MoS_2 FETs, among them the usage of different metals,[25,26] the introduction of an interfacial layer between the metal and semiconductor,[27–29] or the doping of MoS_2.[30,31] Despite significant progresses made over

---

[1] https://irds.ieee.org/roadmap-2017

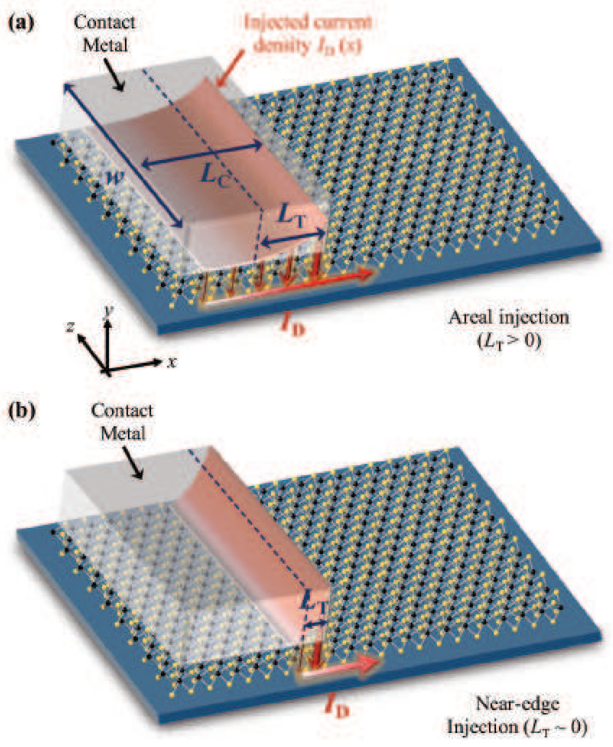
(a)
Contact Metal
Injected current density I_D (x)
w
L_C
L_T
z
y
x
I_D
Areal injection ($L_T > 0$)
(b)
Contact Metal
L_T
I_D
Near-edge Injection ($L_T \sim 0$)

Figure 1: Schematics of top metallic electrodes (gray blocks of width w and length L_C) deposited on 2-D monolayers (atomic structures) with two possible electron injection mechanisms. The behavior of the current density I_D flowing through these heterojunctions is represented by the red surface plots and vertical arrows. (a) Area-dependent injection with a long transfer length L_T. The amount of current penetrating into the 2-D material gradually increases over a metal-semiconductor overlap distance equivalent to L_T along the x-axis (transport direction). (b) Near-edge injection with a close to zero L_T. Almost all electrons are transferred from the contact to the 2-D materials at the edge of the overlap region.

the last few years, metal/MoS$_2$ interfaces have not yet revealed all their secrets, hindering the development of future electronic components based on 2-D materials.

An open issue of critical importance concerns the trajectories followed by electrons leaving a top metal contact and entering a MoS$_2$ monolayer situated underneath. The transfer length L_T, as illustrated in Fig. 1, characterizes the average distance that is needed by carriers to accomplish this transition. No consensus exists on the magnitude of L_T, i.e. on whether the electrical current flows through the metal up to the edge of its interface with MoS$_2$ (edge process, $L_T \simeq 0$) or whether electrons gradually penetrate into MoS$_2$ over a relatively long distance (area-dependent process, large L_T). In the former case, the current would be proportional to the width w of the electrode on MoS_2, whereas in the latter, it would also depend on the contact length L_C, i.e. on the length of the metal/MoS_2 overlap region, provided that $L_C < L_T$. Experimentally, Liu et al.[32] deduced a transfer length of about 600 nm for titanium-connected single-layer MoS_2. Meanwhile, English et al.[33] reported pure Au electrodes on top of bilayer MoS_2 with low contact resistances R_C=740 $\Omega \cdot \mu$m and $L_T \simeq$30 nm, which can be considered a near-edge process.

Obviously, these results are in total contradiction. Various modeling efforts have attempted to identify transfer mechanisms that could explain these opposite trends, but so far without much success. A prominent study relying on density functional theory (DFT), an *ab initio* method, concluded that the transfer of electrons from Ti to MoS_2 should be area-dependent as this 2-D material gets metalized when put in contact with titanium.[23] Another work combining DFT and quantum transport calculations within the framework of the Non-equilibrium Green's Function (NEGF) formalism found that carriers preferably escape the Ti electrode at the edge of the Ti/MoS_2 interface.[34] Finally, device simulations performed in the effective mass approximation suggested that the transfer length increases with the MoS_2 thickness, going from an edge process in monolayers to an area-dependent injection in multi-layer crystals.[35] The apparently contradictory conclusions of these theoretical investigations do not resolve the discrepancies observed experimentally.

To address them, a deeper look at the fabrication of top contacts on 2-D materials should be taken. It has been recently shown that if titanium is deposited on MoS_2 under moderately high vacuum conditions ($\sim 10^{-6}$ mbar), a TiO_2 oxide layer forms at the metal-semiconductor interface. Under ultra-high vacuum ($\sim 10^{-9}$ mbar), this does not happen, allowing the Ti atoms to directly bind to the top S atoms.[36] In this context, the main difference between the results of Refs.[32] and[33] may be the pressure at which the contacts were deposited (moderately high vs. ultra-high vacuum), not the choice of the electrode metal (Ti vs. Au) or the MoS_2 thickness (mono- vs. bi-layer). It is likely that an interfacial oxide layer was present within the Ti/MoS_2 stacks of Ref.,[32] but not within the Au/MoS_2 ones of Ref.[33] The goal of

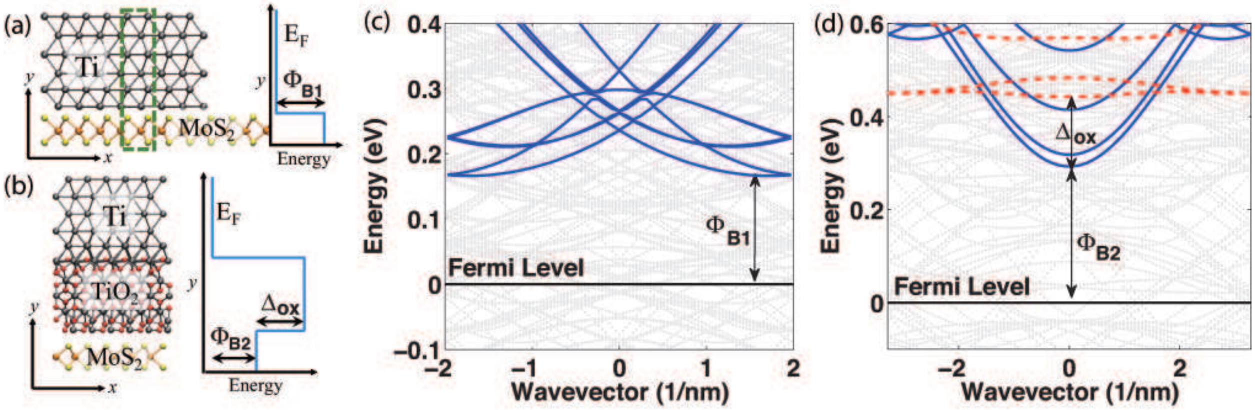

Figure 2: Schematic view of the atomic unit cells of the (a) Ti-MoS_2 and (b) Ti-TiO_2-MoS_2 contact geometries simulated with DFT and used to construct MLWF-based Hamiltonian matrices. The colored spheres represent individual atoms: gray - Ti, red - O, orange - Mo, and yellow - S. The right sub-plots show the corresponding band alignments. In (a), only a small portion of the unit cell is depicted as the real one contains 576 atoms, whereas in (b), the 306 considered atoms are plotted. (c) Electronic bandstructure around the Fermi level E_f=0 eV for the Ti-MoS_2 system. The primitive unit cell delimited by the dashed green rectangle in (a) served as input to this calculation. The dotted gray lines are bands lying within the Ti contacts, blue lines within MoS_2. A Schottky barrier height (SBH) Φ_{B1}=166 meV can be extracted. (d) Same as (c), but for the Ti-TiO_2-MoS_2 unit cell in (b). The dashed red lines refer to the TiO_2 bands. Here, a SBH Φ_{B2}=293 meV was found. The conduction band offset between MoS_2 and TiO_2 was adjusted to Δ_{ox}=150 meV. Because of the different shape of the MoS_2 supercells in (a) and (b), the conduction band minimum of this material in (c) and (d) was not folded to the same *k*-point.

this paper is therefore to analyze the role played by such layers in the contact physics, to determine their influence on the transfer length of electrons at metal/MoS_2 junctions, and to find out whether they can be leveraged to reduce the contact resistance of 2-D devices. To do that, we performed *ab initio* quantum transport simulations and demonstrated that in the absence of an intercalated oxide layer between the top metal contact and MoS_2, the transfer of electrons becomes edge-dependent. Finally, the aforementioned results from the literature are re-examined in light of these findings.

To highlight the impact of an interfacial TiO_2 oxide layer on the electron transfer process, we simulated Ti-contacted single-layer MoS_2 structures, with and without TiO_2 in between, by combining plane-wave DFT, maximally localized Wannier functions (MLWFs), and NEGF.[37] The first step consisted of creating suitable atomic geometries. Since DFT calculations are computationally very demanding, periodic unit cells of the smallest possible dimensions were created, while still large enough to allow for the extraction of the bandstructure and wavefunction of three distinct regions: one with pure Ti, another one made of Ti-(TiO_2)-MoS_2, and a last one containing MoS_2 only. For simplicity, the underlying substrate layer was not included in the DFT study. Atomic configurations fulfilling these conditions are illustrated in Figs. 2(a) and (b). Next, their electronic structure was calculated with the VASP[38] DFT tool within the generalized gradient approximation (GGA) of Perdew, Burke, and Ernzerhof.[39] The single-particle wavefunctions were then transformed into a set of MLWFs with the help of the Wannier90[40] package.

From the chosen unit cells and the produced MLWF Hamiltonian blocks, larger structures with a $\sim$50 nm long free standing MoS_2 part and metal-semiconductor overlap lengths ranging from 6 to 133 nm were constructed following the procedure described in Ref.[41] Even though there is no region with pure Ti in Fig. 2(a) and (b), the influence of MoS_2 and TiO_2/MoS_2 on Ti was found sufficiently weak such that a representative Ti Hamiltonian block could be safely cut off from the generated heterostructures. Similarly, in Fig. 2(b), the penetration of the metal wavefunction into the MoS_2 monolayer was small enough so that the required Hamiltonian blocks of free-standing MoS_2 could be directly derived from the matrix elements of the whole stack. It has been previously verified that the bandstructures of all individual layers (Ti, TiO_2, and MoS_2), computed after the MLWF transformation and the single block extraction, agree well with what is obtained from pure Ti, TiO_2, and MoS_2 unit cells.[41] The results are shown in Figs. 2(c) and (d).

Although DFT is considered a very accurate technique to capture both the conduction (CB) and valence band (VB) states of semiconductors and insulators, it suffers from a well-known band gap underestimation problem. Consequently, the calculated band alignments may not always be reliable. Furthermore, finite size effects may take place in small simulation domains, especially with a random placement of the constituting atoms. This issue was avoided in our DFT calculations, which are limited in size, by replacing amorphous TiO_2 with

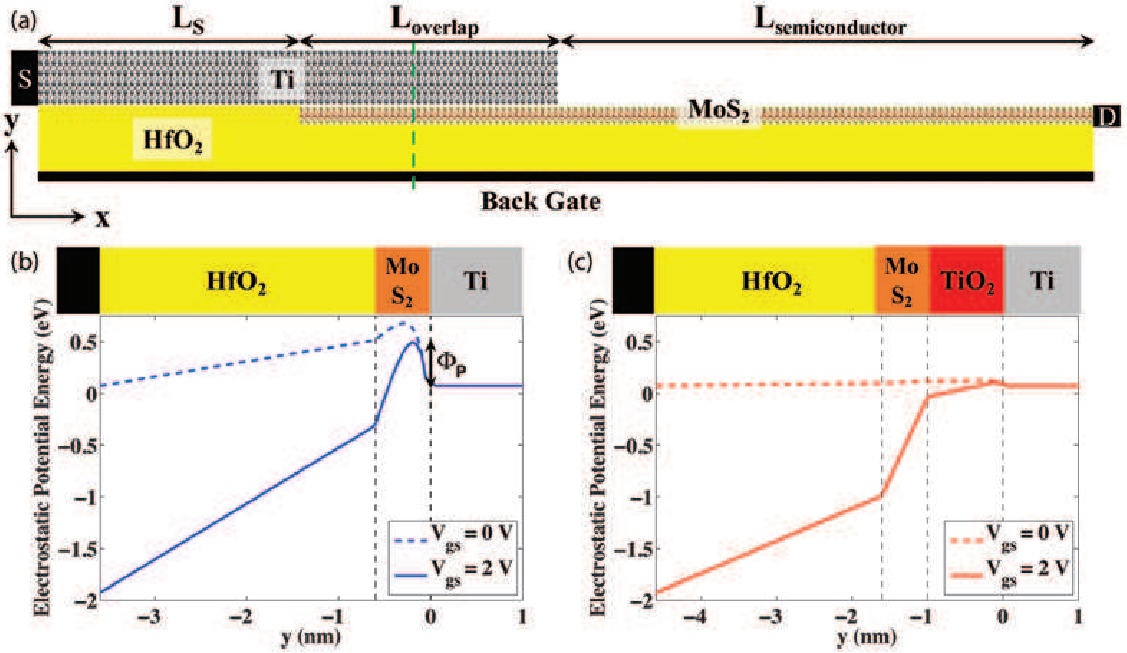

Figure 3: (a) Schematic view of the structures simulated in this work. Ti-(TiO_2)-MoS_2 systems were constructed with a pure Ti region of length L_S=9.5 nm, a Ti-(TiO_2)-MoS_2 overlap region of length 5.7≤ $L_{overlap}$ ≤132.8 nm, and a MoS_2-only region of length $L_{semiconductor}$=47.7 nm. Electrons are injected at the contact labeled S (source) and collected at the one denoted D (drain). The channel is separated from a back gate electrode by a perfectly isolating HfO_2 oxide layer of thickness t_{ox}=3 nm and relative dielectric constant ϵ_R=20. Transport occurs in the x and y directions, the z-axis (out-of-plane) is assumed periodic. (b) Electrostatic potential energy along the vertical dashed green line in (a) at a back gate voltage V_{gs}=0 (dashed line) and 2 V (solid line) for the Ti-MoS_2 contact geometry. The variable Φ_P refers to the bias-dependent potential barrier induced by the Ti contact. (c) Same as (b), but for the Ti-TiO_2-MoS_2 configuration. The TiO_2 layer measures 1 nm in all cases, a value large enough to capture the relevant physics, but thin enough to remain computationally affordable.

its rutile, well-ordered phase. To compensate for this idealization, the TiO_2 CB edge had to be manually raised to 0.15 eV above the MoS_2 one, which corresponds to the experimentally determined band offset.[36] The adjusted band diagram is presented in Fig. 2, where it can also be seen that the non-altered Schottky barrier heights, with (0.29 eV) and without (0.17 eV) TiO_2, are close to the experimental ones (0.23 eV).[42]

After scaling up the Ti-MoS_2 and Ti-TiO_2-MoS_2 unit cells, contact geometries similar to the one shown in Fig. 3(a) were built up and a 3nm thick HfO_2 layer was added to serve as back gate dielectric. The MLWF Hamiltonian matrices of theses systems were inserted into a dissipative NEGF quantum transport solver that returns the current as a function of the applied voltages for a given electrostatic potential.[37] The Green's Functions must be evaluated for all possible electron energy E and momentum k_z pairs before summing up these contributions to give rise to the electron density. To reduce the heavy computational burden associated with NEGF simulations expressed in a MLWF basis, the process was simplified by pre-computing the electrostatic potential with a properly calibrated quantum mechanical solver based on the effective mass picture[43] and by including only one momentum point carrying a representative current density. These approximations, together with the TiO_2 band edge shift, might limit the accuracy of the computed data. Since we focus on a qualitative description of the contact physics, the conclusions of the paper are not affected. More details about the simulation approach can be found in the Supporting Information.

Vertical cuts of the electrostatic potential energy across the Ti-MoS_2 and Ti-TiO_2-MoS_2 heterojunctions are depicted in Figs. 3(b) and (c), respectively, at two different back gate voltages V_{gs}=0 and 2 V. Of particular interest is the response of the MoS_2 monolayer. Without TiO_2, a potential barrier Φ_P of about 0.5 to 0.6 eV forms at the Ti/MoS_2 interface, on top of the already existing Schottky barrier Φ_{B1}=0.166 eV (see Fig. 2). The origin of Φ_P can be traced back to the penetration of the Ti wavefunctions into the MoS_2 band gap, which induces an additional electron density of ∼3e14 cm^{-2} in MoS_2. In Ref.[23] it was inferred that this phenomenon leads to a metallization of MoS_2 and that the created states can carry current, thus causing an area-dependent injection of electrons below the Ti contact. It should however be noted that the electrons within the MoS_2 band gap result from exponentially decaying wavefunctions, with a large imaginary component of their wavevector along all directions. As these carriers cannot propagate, they only marginally contribute to the total current. Hence, speaking of a metallization of the MoS_2 monolayer does not appear justified when the involved electrons are not mobile.[34] The large excess electron density in MoS_2 has nevertheless two important consequences: (i) it pushes up the electrostatic potential energy by Φ_P, which acts as a barrier and blocks the transfer of electrons from the Ti electrode

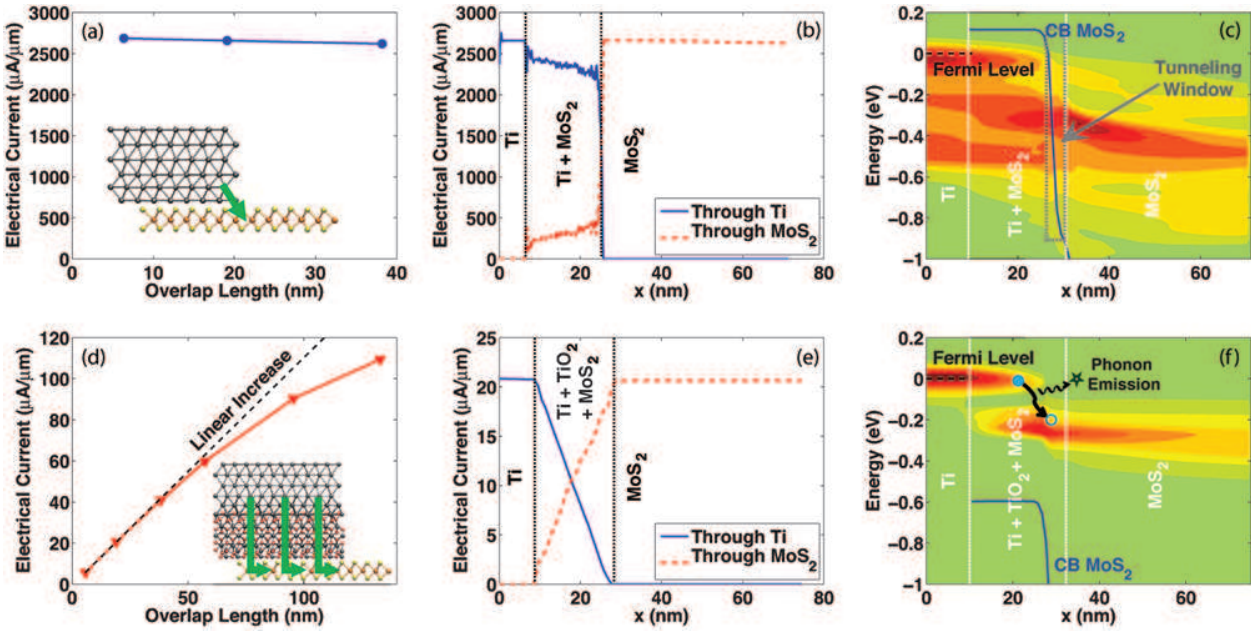

Figure 4: (a) Current flowing through the Ti-MoS_2 contacts in Fig. 3 at V_{gs}=2 V and V_{ds}=2 V as a function of the overlap length $L_{overlap}$. The inset shows that the current (green arrow) is transferred from Ti to MoS_2 at the contact edge. (b) Spatially resolved current along the x-axis in the Ti and MoS_2 regions of the structure with $L_{overlap}$=19.7 nm. An abrupt transfer from Ti to MoS_2 can be observed at the contact edge. (c) Spectral current distribution corresponding to sub-plot (b). Red indicates high current concentrations, green zero current. The blue line refers to the MoS_2 conduction band edge, the dashed line to the Fermi level, and the dashed rectangle, the electron tunneling window. (d-f) Same as (a-c), but for the Ti-TiO_2-MoS_2 contacts. Since the current depends on the metal/MoS_2 overlap length, the whole process becomes area- and no more edge-dependent. This can be best seen by the gradual current transfer between Ti and MoS_2 in (e).

to the MoS_2 layer in the overlap region (high transfer resistance) and (ii) it partly pins the Fermi level of the 2-D channel by screening the influence of the back gate voltage.

The situation is radically different in the presence of an interfacial TiO_2 layer. The oxide prevents the penetration of the Ti wavefunctions into MoS_2 and even depletes the electron population in the overlap region, under flat band conditions. Due to this, the MoS_2 conduction band can be readily modulated by the back gate voltage and pushed below the metal Fermi level, thereby making itself accessible for electrons tunneling through the oxide. This lowers the transfer resistance from Ti to MoS_2. The usage of such Fermi level de-pinning layer has been recently demonstrated for Co/h-BN electrodes.[44]

Using these electrostatic potentials, the current flowing through the assembled Ti-contacted MoS_2 structures was computed at a back gate voltage V_{gs}=2 V and a source-to-drain voltage V_{ds}=2 V measured between the Ti region on the left ("source") and the MoS_2 single-layer on the right ("drain"). Figure 4 unveils the behavior of the electrical current as a function of the (i) metal-semiconductor overlap length $L_{overlap}$, (ii) region where it flows (Ti or MoS_2), and (iii) energy at which it is carried. It clearly appears that when Ti and MoS_2 are in direct contact, the current becomes independent of $L_{overlap}$ and stays constant (Fig. 4(a)). There is almost no current exchange between the top electrode and the bottom 2-D material because of the blocking potential barrier discussed above, except at the edge of the Ti/MoS_2 interface (Fig. 4(b)) where the combined effect of V_{gs} and V_{ds} pushes down the MoS_2 conduction band. This opens up a tunneling window for the electrons situated in the Ti electrode, as can be seen in Fig. 4(c),[34] activating a near-edge injection process whose efficiency hinges on the characteristic (or screening) length λ_c of the contact.[45] Here, due to the ultra-thin bottom HfO_2 layer, λ_c does not exceed 5 nm, but in real devices, it is typically much longer.

The presence of an interfacial TiO_2 layer completely changes the transfer mechanism. The current through the junction linearly increases with the overlap length $L_{overlap}$ before slowly saturating, as reported in Fig. 4(d). By extrapolating this plot, a transfer length L_T ~150 nm can be estimated. Figure 4(e) reveals that the electrical current gradually enters the MoS_2 monolayer from the top metallic contact, over the entire overlap region, which is a clear signature of an area-dependent injection process: the longer the contact, the higher the current magnitude. Although the quantitative I_d values should be taken with precaution because of the applied modeling approximations, in particular the consideration of one single k_z point, the performance of both contact configurations can still be compared to each other. First, it can be observed in Fig. 4(c) that without TiO_2, the current distribution remains fairly homogeneous in the pure Ti and Ti-MoS_2 overlap regions before losing energy when entering the MoS_2-only extension due to phonon emission. When a TiO_2 layer is inserted, phonon-assisted tunneling dominates the Ti-to-MoS_2 electron transfer, as indicated by the current distribution in Fig. 4(f). This trend is confirmed when looking at the ballistic current, which is 2.5 times lower than the one with electron-phonon scattering.

From Fig. 4, it is also apparent that the total injected current is larger without the TiO_2 oxide layer despite the high Ti-MoS_2 transfer resistance caused by the interface potential barrier in the overlap region. This can be explained on one hand by the fact that electrons following the diagonal path shown in the inset of Fig. 4(a) move through a typical Schottky contact whose triangular shape can be modulated by the applied gate-to-source voltage. In this case, a larger characteristic length λ_c, as encountered in real devices, would significantly decrease I_d by making the tunneling distance from Ti to MoS_2 longer. On the other hand, when TiO_2 is present, electrons must tunnel through this oxide to reach the 2-D channel, which reduces the transfer probability. A thinner, more transparent, interfacial layer, e.g. h-BN, could enhance the current magnitude.

It remains to put our work into perspective with literature. As already mentioned above, the metallization of MoS_2 below Ti contacts proposed in Ref.[23] does not support an area-dependence of the electron injection. On the contrary, it pins the Fermi level and deteriorates the modulation of the electrostatic potential in the overlap region. The experimental data of Refs.[32] and[33] agree with our results if we assume that there is a TiO_2 oxide layer between Ti and MoS_2 in the former case, whereas the interface is devoid of any oxide layer in the latter due to the higher vacuum deposition conditions. The modeling-based Ref.[34] postulated a near-edge injection process because a pure Ti-MoS_2 stack (without TiO_2) was simulated. The same was found in Ref.[35] for top contacts on a single-layer of MoS_2. However, the authors of this paper noticed a transition from an edge- to an area-dependent process as the MoS_2 thickness was increased, implying that any interfacial layer could be beneficial as long as it attenuates the penetration of the metal wavefunction into the band gap of the bottom semiconductor layer(s).

In conclusion, we have used *ab initio* simulations to demonstrate that the injection of electrons from a top metallic contact into an underlying 2-D material can occur either at the edge or through the metal-semiconductor overlap area, depending on the presence or not of an interfacial layer. In this paper, Ti electrodes deposited on a MoS_2 layer, with and without an intermediate TiO_2 oxide, have served as an example to illustrate the physics at play. This finding can in principle be generalized to any blocking layer placed at the interface between a top contact and a 2-D monolayer, intentionally or not. Such a layer can hinder the penetration of the wavefunction originating from the metal into the band gap of the semiconductor, thus enabling an area-dependent transfer process. It can be envisioned that by engineering the properties of the interfacial layer the contact resistance of FETs based on 2-D semiconductors could be reduced, for example by selecting a material with a conduction band edge well-aligned with that of the 2-D crystal. Mobile electrons could then be directly injected into the transistor channel, without tunneling. At the same time, the charges pinning the Fermi level would still be stopped by the interfacial layer.

Acknowledgement

This research was supported by ETH Zürich (grant ETH-32 15-1) and the Swiss National Science Foundation und grant no. 200021_165841 and under the NCCR MARVEL. We acknowledge PRACE for awarding us access to Piz Daint at CSCS under Project pr28 and CSCS for Project s876.

Supporting Information Available

The following files are available free of charge. Detailed description of the modeling approach and of the applied approximations.

References

(1) Radisavljevic, B.; Radenovic, A.; Brivio, J.; Giacometti, V.; Kis, A. *Nat Nano* **2011**, *6*, 147–150.

(2) Manzeli, S.; Ovchinnikov, D.; Pasquier, D.; Yazyev, O. V.; Kis, A. *Nature Reviews Materials* **2017**, *2*, 17033.

(3) Qiao, J.; Kong, X.; Hu, Z.-X.; Yang, F.; Ji, W. *Nat. Commun.* **2014**, *5*, 4475.

(4) Liu, H.; Neal, A. T.; Zhu, Z.; Luo, Z.; Xu, X.; Tománek, D.; Ye, P. D. *ACS Nano* **2014**, *8*, 4033–4041, PMID: 24655084.

(5) Mounet, N.; Gibertini, M.; Schwaller, P.; Campi, D.; Merkys, A.; Marrazzo, A.; Sohier, T.; Castelli, I. E.; Cepellotti, A.; Pizzi, G.; Marzari, N. *Nature Nanotechnology* **2018**, *13*, 246–252.

(6) Kuhn, K. J. *IEEE Transactions on Electron Devices* **2012**, *59*, 1813–1828.

(7) Fiori, G.; Bonaccorso, F.; Iannaccone, G.; Palacios, T.; Neumaier, D.; Seabaugh, A.; Banerjee, S. K.; Colombo, L. *Nature Nanotechnology* **2014**, *9*, 768–779.

(8) Baugher, B. W. H.; Churchill, H. O. H.; Yang, Y.; Jarillo-Herrero, P. *Nano Letters* **2013**, *13*, 4212–4216, PMID: 23930826.

(9) Schmidt, H.; Wang, S.; Chu, L.; Toh, M.; Kumar, R.; Zhao, W.; Castro Neto, A. H.; Martin, J.; Adam, S.; Özyilmaz, B.; Eda, G. *Nano Letters* **2014**, *14*, 1909–1913, PMID: 24640984.

(10) Smithe, K. K. H.; English, C. D.; Suryavanshi, S. V.; Pop, E. *Nano Letters* **2018**, *18*, 4516–4522, PMID: 29927605.

(11) Geim, A. K.; Grigorieva, I. V. *Nature* **2013**, *499*, 419–425.

(12) Lee, C.-H.; Lee, G.-H.; van der Zande, A. M.; Chen, W.; Li, Y.; Han, M.; Cui, X.; Arefe, G.; Nuckolls, C.; Heinz, T. F.; Guo, J.; Hone, J.; Kim, P. *Nature Nanotechnology* **2014**, *9*, 676–681.

(13) Iannaccone, G.; Bonaccorso, F.; Colombo, L.; Fiori, G. *Nature Nanotechnology* **2018**, *13*, 183–191.

(14) Yoon, Y.; Ganapathi, K.; Salahuddin, S. *Nano Letters* **2011**, *11*, 3768–3773, PMID: 21790188.

(15) Allain, A.; Kang, J.; Banerjee, K.; Kis, A. *Nature Materials* **2015**, *14*, 1195–1205.

(16) Cheng, Z.; Price, K.; Franklin, A. D. *IEEE Transactions on Electron Devices* **2018**, *65*, 4073–4083.

(17) Kappera, R.; Voiry, D.; Yalcin, S. E.; Branch, B.; Gupta, G.; Mohite, A. D.; Chhowalla, M. *Nature Materials* **2014**, *13*, 1128–1134.

(18) Leong, W. S.; Luo, X.; Li, Y.; Khoo, K. H.; Que k, S. Y.; Thong, J. T. L. *ACS Nano* **2015**, *9*, 869–877, PMID: 25517793.

(19) Guimarães, M. H. D.; Gao, H.; Han, Y.; Kang, K.; Xie, S.; Kim, C.-J.; Muller, D. A.; Ralph, D. C.; Par k, J. *ACS Nano* **2016**, *10*, 6392–6399, PMID: 27299957.

(20) Chai, Y.; Ionescu, R.; Su, S.; Lake, R.; Ozka n, M.; Ozkan, C. S. *physica status solidi (a)* **2016**, *213*, 1358–1364.

(21) Wang, L.; Meric, I.; Huang, P. Y.; Gao, Q.; Gao, Y.; Tran, H.; Taniguchi, T.; Watanabe, K.; Campos, L. M.; Muller, D. A.; Guo, J.; Kim, P.; Hone, J.; Shepard, K. L.; Dean, C. R. *Science* **2013**, *342*, 614–617.

(22) Jain, A.; Szabó, Á.; Parzefall, M.; Bharadwaj, P.; Taniguchi, T.; Watanabe, K.; Luisier, M.; Novotny, L. *arXiv e-prints* **2019**, arXiv:1902.05506.

(23) Kang, J.; Liu, W.; Sarkar, D.; Jena, D.; Banerjee, K. *Phys. Rev. X* **2014**, *4*, 031005.

(24) Guo, Y.; Liu, D.; Robertson, J. *ACS Applied Materials & Interfaces* **2015**, *7*, 25709–25715, PMID: 26523332.

(25) Das, S.; Chen, H.-Y.; Penumatcha, A. V.; App enzeller, J. *Nano Letters* **2013**, *13*, 100–105, PMID: 23240655.

(26) Kang, J.; Liu, W.; Banerjee, K. *Applied Physics Letters* **2014**, *104*, 093106.

(27) Cui, X. et al. *Nano Letters* **2017**, *17*, 4781–4786, PMID: 28691487.

(28) Kaushik, N.; Karmakar, D.; Nipane, A.; Karande, S. h.; Lodha, S. *ACS Applied Materials & Interfaces* **2016**, *8*, 256–263, PMID: 26649572.

(29) Kim, Y.; Kim, A. R.; Yang, J. H.; Chang, K. E.; Kwon, J.-D.; Choi, S. Y.; Park, J.; Lee, K. E.; Kim, D.-H.; Choi, S. M.; Lee, K. H.; Lee, B. H.; Hahm, M. n. G.; Cho, B. *Nano Letters* **2016**, *16*, 5928–5933, PMID: 27552187.

(30) Fathipour, S.; Li, H.; Remskar, M.; Yeh, L.; Tsai, W.; Lin, Y.; Fullerton-Shirey, S.; Seabaugh, A. *Proceedings of the 2016 International Symposium on VLSI Technology, Systems and Application (VLSI-TSA)* **2016**, 1–2.

(31) McDonnell, S.; Addou, R.; Buie, C.; Wallace, R. o. M.; Hinkle, C. L. *ACS Nano* **2014**, *8*, 2880–2888, PMID: 24484444.

(32) Liu, H.; Si, M.; Deng, Y.; Neal, A. T.; Du, Y.; Najmaei, S.; Ajayan, P. M.; Lou, J.; Ye, P. D. *ACS Nano* **2014**, *8*, 1031–1038, PMID: 24351134.

(33) English, C. D.; Shine, G.; Dorgan, V. E.; Saraswat, K. C.; Pop, E. *Nano Letters* **2016**, *16*, 3824–3830, PMID: 27232636.

(34) Luisier, M.; Szabo, A.; Stieger, C.; Klinkert, C.; Brück, S.; Jain, A.; Novotny, L. *Proceedings of the 2016 IEEE International Electron Devices Meeting (IEDM)* **2016**, 5.4.1–5.4.4.

(35) Arutchelvan, G.; Lockhart de la Rosa, C. J.; Matagne, P.; Sutar, S.; Radu, I.; Huyghebaert, C.; De Gendt, S.; Heyns, M. *Nanoscale* **2017**, *9*, 10869–10879.

(36) McDonnell, S.; Smyth, C.; Hinkle, C. L.; Wallace, R. M. *ACS Applied Materials & Interfaces* **2016**, *8*, 8289–8294, PMID: 26967016.

(37) Szabó, A.; Rhyner, R.; Luisier, M. *Phys. Rev. B* **2015**, *92*, 035435.

(38) Kresse, G.; Furthmüller, J. *Phys. Rev. B* **1996**, *54*, 11169–11186.

(39) Perdew, J. P.; Burke, K.; Ernzerhof, M. *Phys. Rev. Lett.* **1996**, *77*, 3865–3868.

(40) Mostofi, A. A.; Yates, J. R.; Lee, Y.-S.; Souza, I.; Vanderbilt, D.; Marzari, N. *Computer Physics Communications* **2008**, *178*, 685 – 699.

(41) Szabo, A. Dissipative quantum transport simulations in two-dimensional semiconductor devices from first principles. Ph.D. thesis, ETH Zürich, 2016.

(42) Kim, C.; Moon, I.; Lee, D.; Choi, M. S.; Ahmed, F.; Nam, S.; Cho, Y.; Shin, H.-J.; Park, S.; Yoo, W. J. *ACS Nano* **2017**, *11*, 1588–1596, PMID: 28088846.

(43) Luisier, M.; Schenk, A. *IEEE Transactions on Electron Devices* **2008**, *55*, 1494–1501.

(44) Cui, X. et al. *Nano Letters* **2017**, *17*, 4781–4786, PMID: 28691487.

(45) Appenzeller, J.; Knoch, J.; Bjork, M. T.; Riel, H.; Schmid, H.; Riess, W. *IEEE Transactions on Electron Devices* **2008**, *55*, 2827–2845.